High-Resolution Molecular Gas Temperatures in the Galactic Center Cloud M0.10-0.08

Genna Crom[1] and Dr. Natalie Butterfield[2]

[1] *Department of Physics and Astronomy, University of Iowa, 30 North Dubuque St, Iowa City, IA 52242, USA*
[2] *Green Bank Observatory, 155 Observatory Rd, PO Box 2, Green Bank, WV 24944, USA*

Abstract

We present high resolution ($\sim 1''$, 0.01 pc) rotational and kinetic gas temperature measurements of the Galactic center cloud M0.10-0.08, or the 'Sticks' cloud. The Sticks cloud is a compact ($\sim 100''$, 3 pc) cloud $\sim$25 pc in projection of the supermassive black-hole SrgA*. Using multiple transitions of NH_3 taken with the Very Large Array (VLA) radio interferometer, we derive gas temperatures throughout the cloud using two methods: a temperature map and a Boltzmann plot distribution. Our analysis shows warm gas temperatures ranging from 200-500 K with spots up to 800 K. These high resolution gas temperature measurements are warmer than low resolution studies (e.g., Krieger et al., 2017).

1 Introduction

The molecular gas in the inner 500 parsecs of the Galactic center is defined as the Central Molecular Zone (hereafter, CMZ). Several clouds in the CMZ have high densities on the order of 10^5 cm^{-3} (Zylka et al., 1992), compared to the clouds in the Galactic disk which have densities of around 10^{2-3} cm^{-3} (Mills et al., 2018). The molecular gas in the CMZ also has warmer temperatures of 40−200 K (Krieger et al., 2017) than gas in the Galactic disk (10−20 K). These warmer gas temperatures are seen throughout the CMZ, across large size scales (1−10 pc; Krieger et al., 2017, Ginsburg et al., 2016). However, the heating mechanism that is producing this hotter gas is not well understood. There are two leading theories behind this heating mechanism: cosmic ray heating (Yusef-Zadeh et al., 2013) and shock heating (Gisburg et al., 2016). Further, the environmental conditions observed in the CMZ have been shown to be similar to the gas conditions seen in galaxies of high red-shifts (z=2−3; Kruijssen et al., 2013). At these large distances, however, current telescope capabilities are unable to resolve individual clouds. Therefore, the CMZ is thought to be a local analog which could allow us to study these properties at high resolutions.

Observing the CMZ can be challenging due to the Galactic disk. Many wavelengths such as optical and UV, that are produced in the CMZ and the extended Galactic center, are obscured due to the high column densities of interstellar dust in the Galactic disk. Therefore, longer wavelengths, which have longer path lengths, such as radio waves, are used to observe the CMZ. Another challenge is caused by source confusion from multiple components along the same line-of-sight in the Galactic disk. It is difficult to untangle which measurements belong to which cloud, and what the distance of that cloud is from the Galactic center. For example, an observation made with CO have proved to be challenging because of how ubiquitous CO is in the Galactic disk. Observations of ammonia (NH_3), however, may be a better tracer of gas in the CMZ.

NH_3 has a high critical density of 10^{3-7} cm^{-3} (Ott et al., 2014) that is similar to the densities seen in the Galactic center. This means that NH_3 will only form in regions that are at least that dense. Therefore, observations made with

NH_3 will only trace the extended CMZ rather than the Galactic disk that has densities lower than the critical density of NH_3. Previous NH_3 surveys have found that the CMZ (i.e., the inner 3.5°) accounts for around 80 percent of the integrated NH_3 (1,1) emission between Galactic longitudes 290° to 30° (Longmore et al., 2013; see their Figure 1). This result highlights the usefulness of NH_3 as a tracer of the CMZ.

NH_3 is also known to be a good thermometer, with inversion lines that cover rotational temperatures from close to absolute zero to thousands of Kelvin (Krieger et al., 2017). The metastable rotational transitions of NH_3 (where J=K) are known to have longer lifetimes of 10^9 seconds (∼30 years; Ho & Townes, 1983a), and therefore are able to be populated before dropping down in energy level and releasing photons. This makes the metastable transitions particularly useful for detecting more diffuse structures.

We aim to investigate high-resolution (3″; ∼0.1 pc) temperature fluctuations in the CMZ cloud M0.10-0.08, also known as the Sticks cloud. The Sticks cloud is a part of a group of three clouds called the Three Little Pigs, which also include the Straw (M0.145-0.086) and Stone (M0.068-0.075) clouds. These clouds are located ∼20 pc, in projection, from the supermassive black hole Sgr A*, and are thought to represent different evolutionary stages of star formation (Battersby et al., 2017).

2 Observations

The observations used in this analysis focused on a single pointing from a larger survey (VLA11B-210). The larger survey was observed over two days (January 13−14, 2012), taken with the K band (18.0−26.5 GHz) and Ka band (26.5−40 GHz) receivers using the hybrid DnC array of the Karl G. Jansky Very Large Array (hereafter, VLA). With the exception of (8,8), we observed the metastable NH_3 transitions (1,1) through (9,9) which have rest frequencies spanning from 23.8701 to 27.4779 GHz. Our images had spectral resolutions of 1.58−3.14 km s^{-1}, and a sensitivity of ∼1 mJy $beam^{-1}$ per channel. All images were smoothed from their natural resolution to a 3″ by 3″ beam size using the CASA task IMSMOOTH. We also regridded (using the CASA task IMREGRID) each smoothed image with the NH_3 (4,4) smoothed image as a template as it was the smallest shape of [278, 152] pixels.

3 Results

NH_3 is well known for its ability to measure gas temperatures in the CMZ (e.g., Longmore et al., 2013, Mills et al., 2018). The multiple transitions of NH_3 in this study will allow us to measure the rotational and kinetic gas temperatures in the M0.10-0.08 cloud. In order to calculate the temperature of the M0.10-0.08 cloud, we first converted from units of flux density to brightness temperature using the following equation:

$$T_B(K) = \frac{1.224 \times 10^6}{\theta_{\rm min}\theta_{\rm max}} \Big(\frac{S_\nu}{\rm Jy}\Big) \Big(\frac{\nu}{\rm GHz}\Big)^{-2} \quad (1)$$

where S_ν is the flux density in units of Jy at a frequency ν in GHz. $\theta_{\rm min}$ and $\theta_{\rm max}$ are the convolved restoring beam in arcseconds and T_B is the resulting brightness temperature in Kelvin.

After converting the emission from units of Jy to K, we must then calculated the column density (N), in units of cm^{-2}, using the following equation:

$$\rm N(J,K) = \frac{J(J+1)}{K^2} \frac{1.55 \times 10^{14}\ cm^{-2}}{\nu} \int T_B dv \quad (2)$$

where $\int T_B dv$ is the velocity integrated brightness temperature, ν is the rest frequency of the transition, and J and K are the rotational quantum numbers.

Finally, we calculate the rotational temperature $T_{JJ'}$ between two transitions using the following equation:

$$\frac{N_u(J',K')}{N_u(J,K)} = \frac{g_{\rm op}(J')}{g_{\rm op}(J)} \frac{2J'+1}{2J+1} exp\Big(\frac{-\Delta E}{T_{\rm JJ'}}\Big) \quad (3)$$

where the left hand side is the ratio of the column density (N_u) in between two transitions (derived in Equation 2), $g_{\rm op}$ is the statistical weight of the ortho (J=3n; $g_{\rm op}$=2) and para (J≠3n; $g_{\rm op}$=1) transitions, and ΔE is the difference in energy levels, in units of K, between the two transitions.

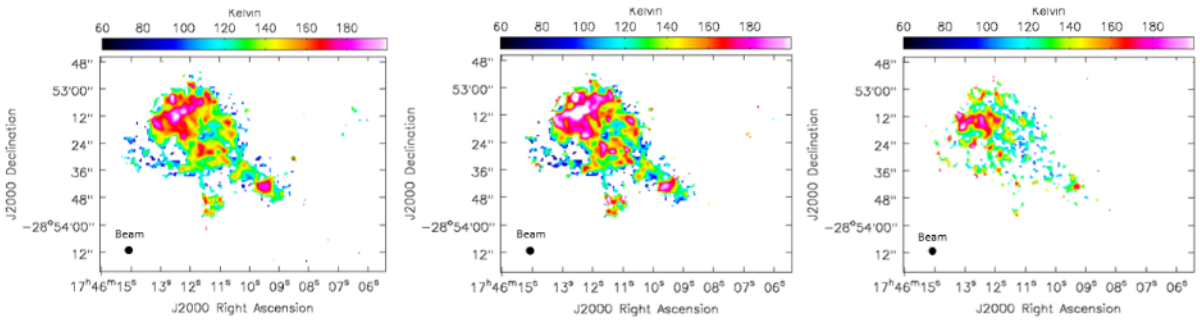

Figure 1: (left) Rotational T_{47} temperature map created using the NH_3 (4,4) and (7,7) para transitions, (center) Rotational T_{57} temperature map created using the NH_3 (5,5) and (7,7) para transitions. (right) Rotational T_{69} temperature map created using the NH_3 (6,6) and (9,9) ortho transitions.

In the following sections, we will measure the high-resolution gas temperature of M0.10-0.08 using two different approaches. In the first method we will use two pairs of transitions to create a gas temperature map which calculated a temperature value for every pixel (Section 3.1). The second method will be using multiple transitions to measure gas temperature across an integrated region (Section 3.2). We will then compare the two methods for consistency checks in Section 3.3.

3.1 Creating Temperature Maps

The first method creates a temperature map using the data cubes of two metastable (J=K) transitions. We first convert the data cubes from Jy to K using Equation 1 and the CASA task IMMATH. We then integrate the brightness temperature over a velocity range of 35−70 km s^{-1}, moment 0 in the CASA task IMMOMENTS, to produce the $\int T_B dv$ in Equation 2. We then used the CASA task IMMATH again, along with the moment 0 images, to create the column density map for each transition using Equation 2. Finally, we take the ratio of the two column density maps and use the CASA task IMMATH to solve for the rotational temperature in Equation 3.

The resulting rotational temperature maps for the T_{47}, T_{57} and T_{69} transitions are shown in Figure 1 and the temperature map for the T_{45} transition is shown in Figure 2 (top). These rotational temperature maps show gas temperatures ranging from 60 to 180 K. Most of hot gas (T > 150 K) is located towards the center of the cloud with a warmer clump near the south-east side of the cloud (near RA=$17^h46^m09.5^s$; Dec=-28°53′48″). The rotational temperature for the (4,4) and (5,5) transitions is shown in Figure 2 (top). We calculated the kinetic temperature for the T_{45} rotational temperature map using conversions (described in Table 1) from Ott et al., (2011). The kinetic temperature map for the (4,4) and (5,5) transitions is shown in Figure 2 (bottom). The kinetic temperature is shown to have a larger range of temperatures compared to the rotational temperature map (Figure 2), with temperatures ranging from ∼100−700 K. This higher gas temperature in the kinetic temperature map compared to the rotational temperature map is expected as the rotational temperature map is a lower limit of the gas temperature (e.g., Ott et al., 2011).

Table 1: Conversion equations for the rotational to kinetic temperature conversion obtained from Ott et al., (2011).

	Conversion Equations	**T_{kin} Range (K)**
$\mathbf{T_{kin,45}}$=	$1.143T_{rot,45} - 1.611$	0−50
	$21.024T_{rot,45} \times e^{0.0198}$	50−500

3.2 Creating Boltzmann Plots

The second approach creates a Boltzmann plot using all of the data cubes of the observed metastable transitions (4,4)−(7,7) & (9,9) (see Section 3.3 for exceptions). Similar to the first approach, we start out by converting the data

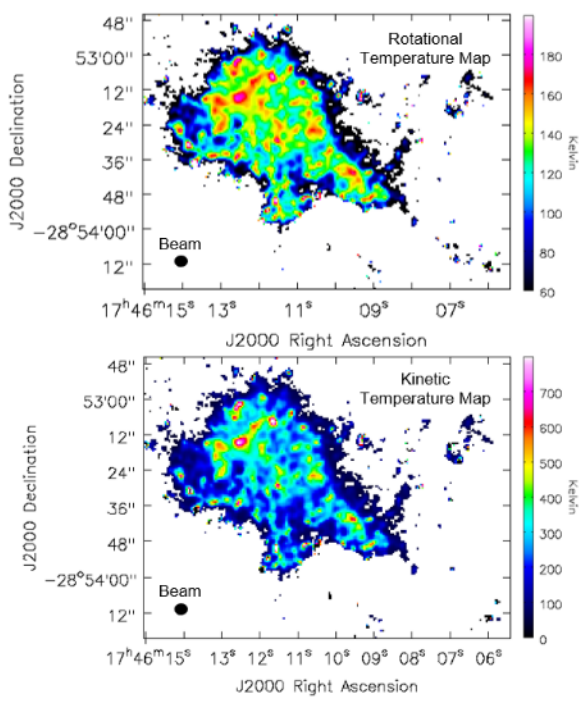

Figure 2: Rotational T_{45} (top) temperature map created using the NH_3 (4,4) and (5,5) transitions. Kinetic T_{45} (bottom) temperature map created using the conversion equation in Table 1.

cubes from Jy to K using Equation 1, however, in this method we use the Python package *Astropy* to do the conversion. Our code then averages the values in a predefined circular region and extracts a spectra for each data cube. These spectra are created using the Python package *Pyspeckit* (Ginsburg & Mirocha 2011) and are represented as brightness temperature (T_B) vs velocity (km s^{-1}) histogram plots. The velocity axis is a different representation of how far in frequency the emission is from the rest frequency of the rotational transition.

Next, we calculate the column density for each data cube using Equation 2, where the integral of the fitted Gaussian now takes the place of the moment 0 map (or $\int T_B d\nu$).

After the column densities have been calculated for each data cube, we then plot the log of the column density vs the energy of each transition. The inverse slope of the best fit line to this plot is the temperature, creating what is known as a Boltzmann plot (see Figure A.2). These Boltzmann plots have been used to calculate temperatures in numerous CMZ clouds (e.g., Mills & Morris, 2013). We still use Equation 3 in the second approach, but here we solve for temperature using a graphing solution. This approach allows us to use many data points (i.e. transitions) instead of only two (see Section 3.3 for further discussion).

3.2.1 Temperature Calculations of M0.10-0.08 Regions

Since the Boltzmann plot approach uses the integrated spectra to measure temperature, we must first define regions in our cloud. We defined our regions to be circular apertures centered around a spot that was significantly hotter or colder than the rest of the cloud. We used the (4,4)-(5,5) temperature map as a template to define our regions so that we can compare them with the previous maps (see Figure 4).

Figure A.2 shows the Boltzmann plots for regions A-F. We measure rotational temperatures from ∼170 K- 224 K. Compared to the temperature map approach, the temperatures derived in the Boltzmann plot approach were higher. For example, region A had a rotational temperature 150K in the temperature map approach, where as the Boltzmann plot for region A shows a temperature of 224 K.

3.2.2 Variations in Temperature as a Function of Radius

As described in Section 3.2, our python code uses predefined circular regions (in a CASA region file). We wanted to test how the size of our regions could effect the temperature measurements in our Boltzmann plot. In order to test this, we defined five regions varying in size centered on the same clump (see Figure 3). We then calculated the temperature of each region using the method described in Section 3.2. The region sizes are $\frac{2}{3}\times$, $\frac{5}{6}\times$, $1\times$, $2\times$, and $3\times$ the $3''$ diameter circular beam (described in Table 2).

The calculated gas temperatures span from 222.82 K to 236.95 K, a range of ∼14 K. While 14 K can seem quite large, with respect other high gas temperatures we measure in this cloud, this error estimate only results in a ∼6% variation in the rotational temperature measurement.

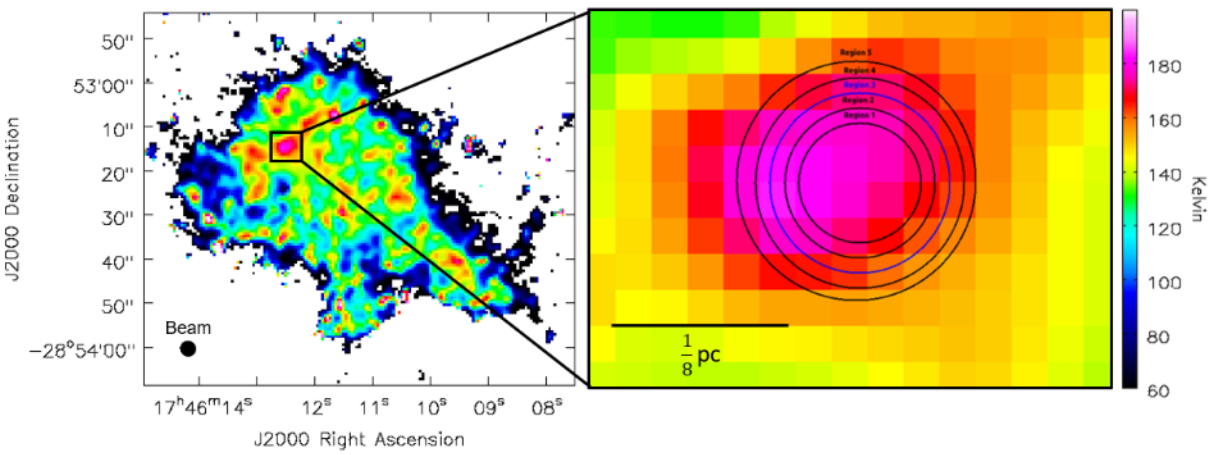

Figure 3: (Left) T_{45} temperature map from Figure 2. (Right) Zoomed in image of the temperature map of the black box in (left). Overlaid are the 5 regions discussed in Section 3.2.2 and Table 2. The middle region (region 3) has the same diameter as the convolved beam (3″).

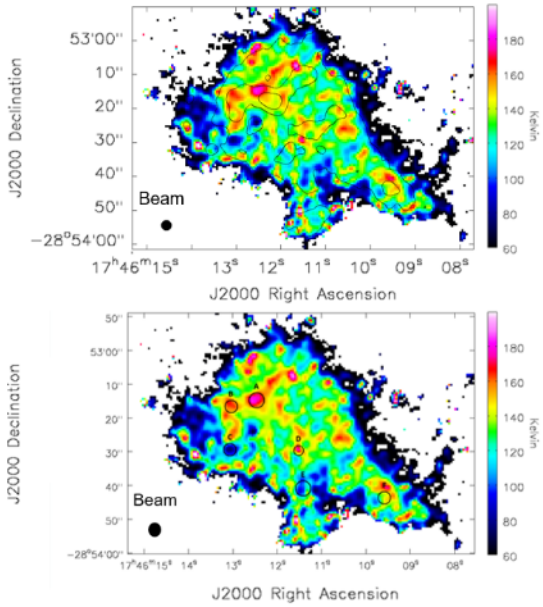

Figure 4: (Top) The (4,4)−(5,5) temperature map with black contours corresponding to the moment 8 map, with contours at 5, 10, 15σ (2.4 mJy beam^{-1}). (Bottom) The regions we defined (labeled A−F) overlaid on the (4,4)−(5,5) temperature map.

3.3 Advantage and Drawbacks

In this section we will compare the advantages and drawbacks of the two methods discussed above. The temperature map approach, described in Section 3.1, allows for a pixel-by-pixel analysis and can show temperature fluctuations across the cloud. However, this approach is only able to use two data points, or transitions, at once. Further, the individual pixel values may not be reliable at our resolution and may need to be further smoothed. There are also often "hot pixels" around the edges of our temperature maps. These hot pixels are caused by a discrepancy in the diffuse emission in that pixel between the two transitions.

The Boltzmann Plot approach, discussed in Section 3.2, averages over a designated region rather than calculates individual pixels. This method allows for a more reliable temperature calculation of that entire region, as it is able to use as many data points, or transitions, in the calculation. One drawback of this method is having to manually produce these plots and calculate temperatures for each region. There may also be information lost when we average over the region and extract a spectra. For example, a small portion of hot gas within a larger region would be averaged out by the extended colder gas. Another drawback is that as we add more transitions, there may be multiple fits possible and thus multiple temperature derivations.

4 Discussion

In the following sections we will discuss our results in the larger context of the Galactic center science and compare our results with other observational studies.

4.1 High Resolution Temperature fluctuations vs Large-Scale Temperature Surveys

The SWAG survey found that the M0.10-0.08 cloud kinetic temperature T_{45} ranges from around 40 K to 120 K (Krieger et al., 2017). We measure large-scale gas temperatures to be around 100 K to 200 K, which agrees with the Krieger et al. (2017) findings. However, when we observed the gas on higher resolution scales ($\sim 1''$), we measure kinetic temperatures ranging from 200 to 500 K, with hot spots up to 800 K (see bottom image in Figure 2). This could mean that there is some systematic effect going on that shows lower NH_3 temperatures with lower resolution observations of these regions. However, this conclusion requires further testing.

4.1.1 1.3 mm Dust Cores and Dense Gas Tracers

Within molecular clouds, regions with higher densities of dust are called dust cores and are the beginnings of star formation if the gravitational forces within the molecular cloud are enough to cause the dust to collapse. These dust cores absorb the emission of background starlight and emit thermal radiation in the infrared, millimeter, and sub millimeter wavelengths.

Figure 5 shows the 1.3mm dust from recent SMA observations of the Sticks cloud (Battersby et al., 2020) in contours overlaid on our rotational temperature map created with NH_3 (4,4) and (5,5) transitions. The resolution of the SMA observations is $\sim 3.5''$ which is comparable to our temperature maps shown in Figure 1 and 2 ($3''$ resolution). They detect 2 main cores at (0.1074, -0.0845) and (0.0957, -0.0796), which overlap with our regions A and F, respectively.

Table 2: Region Sizes centered around $17^h46^m12.453^s$, $-28°53'14.712''$ (region A).

Region	Radius (arcseconds)	T_{rot} (K)
1	1.00	235.95
2	1.25	236.35
3	1.50	236.40
4	1.75	230.97
5	2.00	222.82

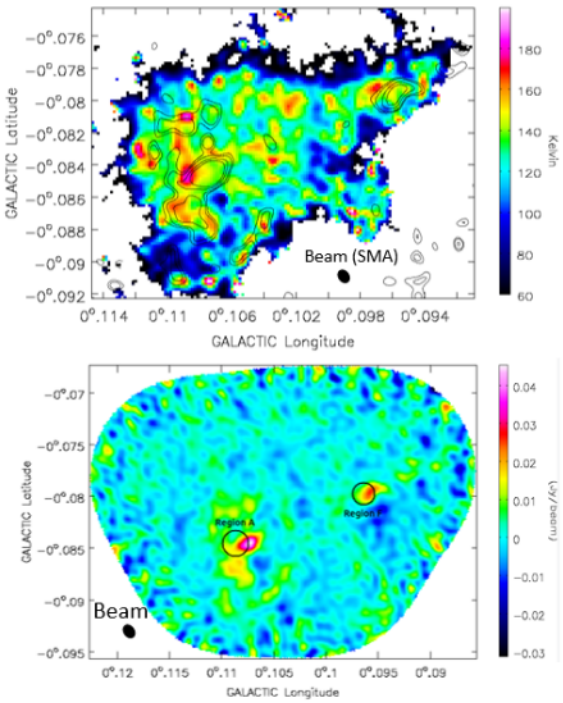

Figure 5: (Top) Temperature map created with NH_3 (4,4) and (5,5) transitions (Figure 2) with 1.3 mm dust emission from the SMA overlaid in black contours at 3, 4, 6, and 8σ (2.5 mJy beam^{-1}). (Bottom) The 1.3mm dust emission from the SMA with our regions A and F shown in black.

The dust cores seem to correspond moderately well with our defined regions, with both regions within $\sim 29''$ ($\sim$1.2 pc), at a distance of 8 kpc to the Galactic center, of the center of the 1.3mm emission. When the dust cores are compared instead to the NH_3 (4,4) moment 8 map (as seen in contours in Figure 5), the center of the region less than $\sim 3''$, or $\sim$0.08 pc, from the center of the 1.3mm emission. This may indicate that it is better to use moment 8 maps (or maximum value maps) instead of temperature maps for future region definitions. We measure temperature values in region A and F to be 223.643 K and 187.474 K.

Dense gas tracers such as CH_2CN generally trace the bright dust regions. Figure 6 shows our temperature map created with NH_3 (4,4) and (5,5) transitions (Figure 2) with ALMA CH_2CN observations overlaid in black

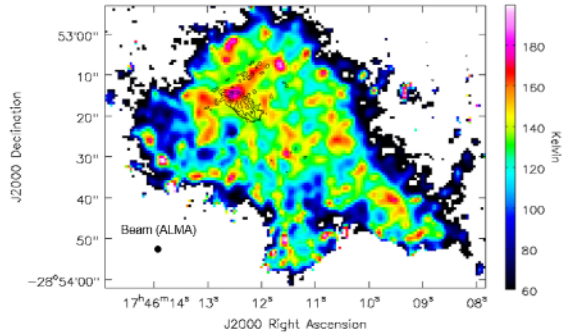

Figure 6: Rotational temperature map created with NH_3 (4,4) and (5,5) transitions (Figure 2) with ALMA CH_2CN observations overlaid in black contours at 3, 4, 6, and 8σ (7.39 mJy beam^{-1}).

Table 3

Star	RA (J2000)	Dec (J2000)	Spectral Type
1	17:46:02.62	-28:54:14.2	WC9
2	17:46:10.03	-28:55:32.5	WN8–9h
3	17:46:17.58	-28:53:03.8	WN8–9h

contours. The ALMA observations were at 3mm and had a restoring beam of 1.36″ by 1.15″. The CH_2CN emission is averaged using three transitions of CH_2CN: 5(1,4)−4(1,3) (J=9/2-7/2), 5(1,4)−4(1,3) (J=11/2-9/2) and 5(1,5)−4(1,4) (J=11/2-9/2). The CH_2CN emission is concentrated towards the center of the cloud and overlaps with some of the hottest gas detected in the cloud (i.e., Region A).

4.1.2 Isolated Massive Stars

Mauerhan et al., (2010) identifies 19 isolated massive stars, or stars with no spatial association known stellar clusters, near the Galactic center region using Paschen-α emission-line excess (the n=4−3 transition of Hα) from the Hubble Space Telescope. Of the 19 stars, three are within 2 pc (∼50″) of the Sticks cloud. Table 3 lists the coordinates of these isolated massive stars, as well as their spectral types. These stars are labeled 14, 15, 16, respectively, in the Mauerhan et al., (2010) study. These isolated massive stars would be roughly near the lower right corner, lower-middle, and left-middle areas of our J2000 image grids. Stars 1 and 2 are further off from the cloud, and other than the dust core we identify as Region F, there are no hot spots towards that direction. Star 3, on the other hand, is close to many clumps near the edge of our cloud (Regions A, B, and other hot spots not identified with our regions). This could indicate that star 3 is causing heating on that side of the Sticks cloud, although this would need to be tested further.

4.1.3 No Radio Continuum detected in M0.10-0.08

Although we made observations using the NH_3 rotational transitions, other studies have observed the Sticks cloud in the radio continuum. Figure 2 in Butterfield et al., (2018) shows the 25 GHz radio continuum towards M0.10-0.08. The radio continuum in this region is low ($\leq$0.12 mJy beam^{-1}) compared to other continuum in the observed survey (i.e., the Sickle HII region). The morphology of the radio continuum in the M0.10-0.08 field does not correlate to the molecular emission observed in the M0.10-0.08 cloud suggesting the emission is not associated. The low radio continuum in the cloud suggests it is relatively quiescent and does not contain any embedded star formation. Therefore, the warm gas we observe in the cloud is not likely due to thermal emission from young massive stars.

5 Conclusion

We measure the rotational and kinetic gas temperatures in the Galactic center cloud M0.10-0.08 using multiple transitions of ammonia (NH_3). The high-resolution observations, taken with the VLA, enabled us to observe temperature fluctuations on the 3″ size scales. We measured the gas temperature using two methods. First, we used the temperature map approach, described in Section 3.1, to calculate the temperature value for each pixel in a data cube. We created temperature maps for the para transition pairs (4,4)−(5,5), (4,4)−(7,7), (5,5)−(7,7),and ortho transition pair (6,6)−(9,9). Second, we used the Boltzmann plot approach, described in Section 3.2, to derive a temperature over a specified region. We specified 6 regions (A−F; see Figure

4) and created their corresponding Boltzmann plots (see Figure A.2). Overall, our large scale temperature calculations ($T_{kin,45}$=100−200K) match previous studies. However, our high resolution temperature calculations range are much higher, ranging from 200−500 K with spots up to 800 K.

References

1. Battersby, C., Keto, E., Walker, D., et al. 2020, ApJS, accepted
2. Battersby, C., Keto, E., Zhang, Q., et al. 2017, The Multi-Messenger Astrophysics of the Galactic Centre, 322, 90
3. Butterfield, N., Lang, C.C., Morris, M., Mills, E.A.C., & Ott, J. 2018, ApJ, 852, 11
4. Ginsburg, A., Henkel, C., Ao., Y., et al. 2016, A&A, 586, 31
5. Ginsburg, A., & Mirocha, J. 2011, Astrophysics Source Code Library
6. Ho, P. T. P., & Townes, C. H. 1983, ARA&A, 21, 239
7. Krieger, N. et al. 2017, ApJ, 850, 77
8. Kruijssen, J.M. & Longmore, S.N. 2013, MNRAS, 435, 2598
9. Longmore, S. N. et al. 2013, MNRAS, 429, 987
10. Mauerhan, J. C., Morris, M. R., Cotera, A., Dong, H., Wang, Q. D., Stolovy, S. R., Lang, C., & Glass, I. S. 2010, ApJ, 713, L33
11. Mills, E. A. C., & Morris, M. R. 2013, ApJ, 772, 105
12. Mills, E.A.C., Ginsburg, A., Immer, K., et al. 2018, ApJ, 868, 7
13. Ott, J., Henkel, C., Braatz, J. A., & Weib, A. 2011, ApJ, 742, 95
14. Ott, J., Weiß, A., Staveley-Smith, L., et al. 2014, APJ, 785,55
15. Yusef-Zadeh, F., Cotton, W., Viti, S., Wardle, M., & Royster, M. 2013, ApJL, 764, L19
16. Zylka, R., Guesten, R., Henkel, C., & Batrla, W. 1992, A&AS, 96, 525

A Appendix

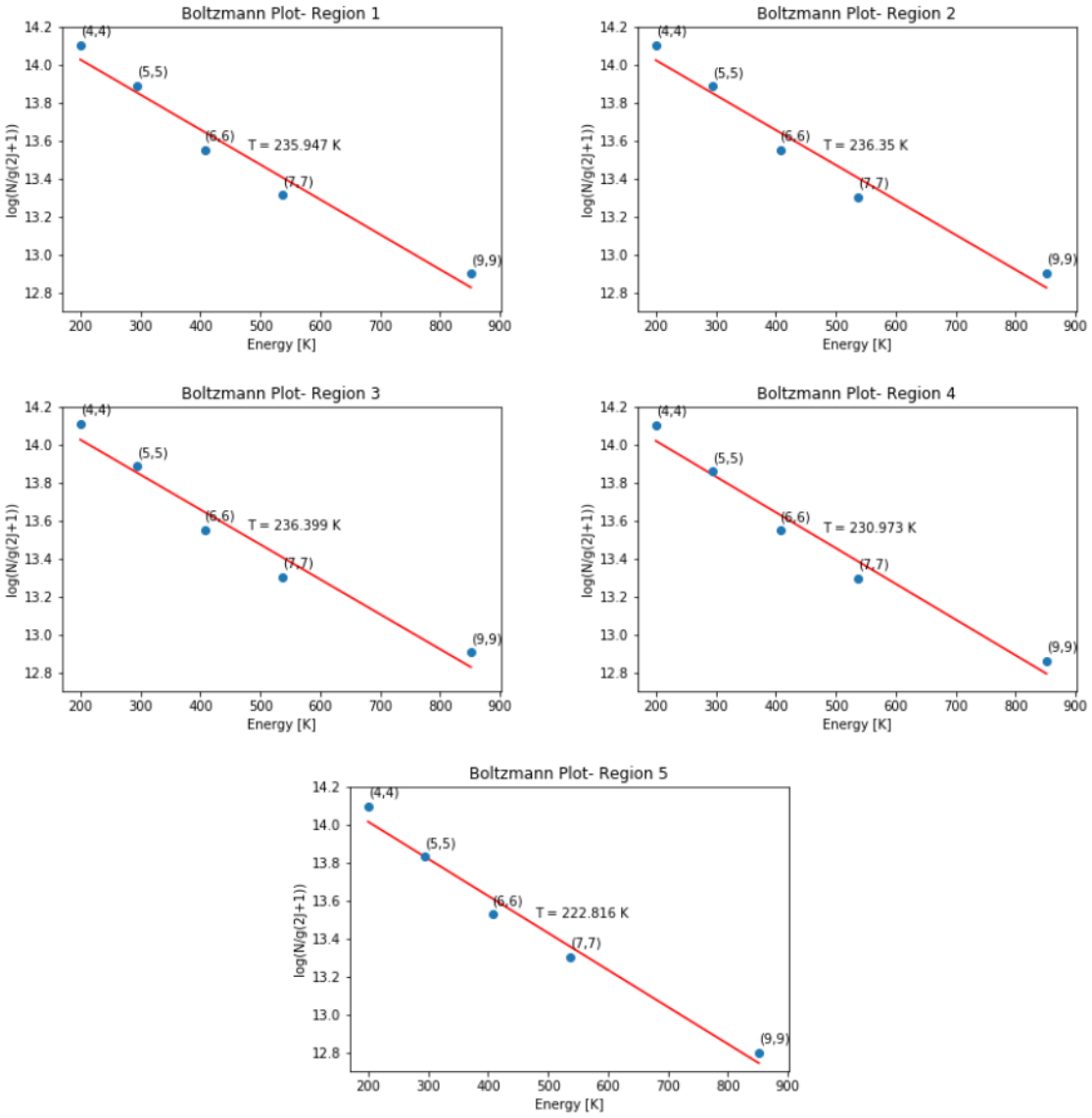

Figure A.1: Boltzmann Temperature Plots for regions 1-5 shown in Figure 3. Each region differs in radii size, as shown in Table 2.

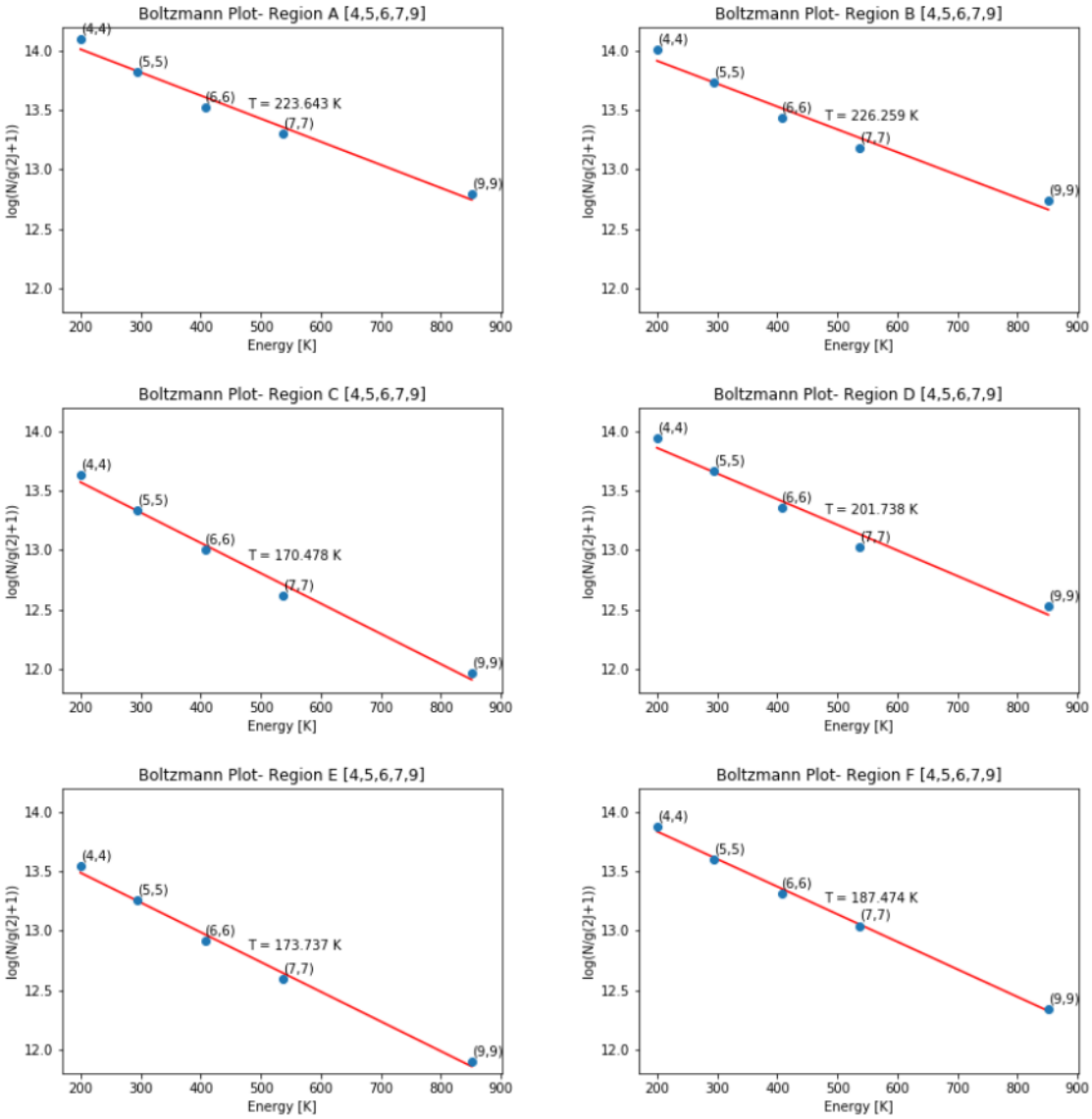

Figure A.2: Boltzmann Temperature Plots showing the column density as a function of energy for the NH_3 (4,4) - (7,7) & (9,9) transitions. The rotational temperature is calculated from the inverse slope of the best fist line for the 5 data points, as discussed in Section 3.2. These regions are labeled A-F based on spatial positions, and are shown in Figure 4.